Journal of Medicinal Chemistry

Brief Article

pubs.acs.org/jmc

Crystallographic and Receptor Binding Characterization of *Plasmodium falciparum* Macrophage Migration Inhibitory Factor Complexed to Two Potent Inhibitors

Georgios Pantouris,[†] Deepa Rajasekaran,[†] Alvaro Baeza Garcia,[‡] Victor G. Ruiz,[†] Lin Leng,[‡] William L. Jorgensen,[§,∥] Richard Bucala,[‡,∥] and Elias J. Lolis*[,†,∥]

[†]Departments of Pharmacology, [‡]Internal Medicine, [§]Chemistry, and the [∥]Yale Cancer Center, Yale University, New Haven, Connecticut 06520-8066, United States

Supporting Information

ABSTRACT: We report the crystal structures of two inhibitors of *Plasmodium falciparum* macrophage migration inhibitory factor (*Pf*MIF) with nanomolar K_i's, analyze their interactions with the active site of *Pf*MIF, and provide explanations regarding their selectivity of *Pf*MIF versus human MIF. These inhibitors were also found to selectively inhibit interactions between *Pf*MIF and the human MIF receptor CD74. The results of this study provide the framework for the development of new therapeutics that target *Pf*MIF.

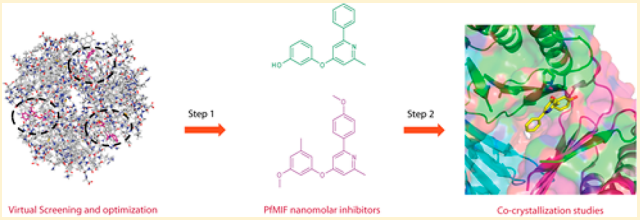

INTRODUCTION

About 300 million people live with malaria due to infection by *Plasmodium falciparum*, which causes over 500000 deaths per year, predominantly in infants. Although advances have been made to limit and treat infections, many strains have developed resistance to current drugs and threaten individuals in developing countries where malaria is an epidemic.[1] *Plasmodium falciparum* macrophage migration inhibitory factor (*Pf*MIF) is a homologue of the human protein that induces inflammation, is expressed in all stages of the parasite's life cycle, and disrupts the emergence of an appropriate memory T-cell response.[2]

The structures of *Pf*MIF[3] and the human MIF (hMIF) homotrimer[4−6] resemble two microbial enzymes, 4-oxalocrotonate tautomerase (4-OT) and 5-carboxymethyl-2-hydroxymucanate (CHM) isomerase,[7] that use an N-terminal proline located between subunits as a catalytic base.[8] Proline is also present at the N-terminus of *Pf*MIF, is conserved among MIF cDNAs from *Caenorhabditis elegans* to humans, and has an unusually low pK_a of 5.6 in hMIF that is consistent with a function as a catalytic base. Human MIF resides in the cytosol[9] until it is exported when cells become activated.[10,11] Extracellular MIF functions by binding its receptor CD74 and recruiting the signaling subunit CD44 to the MIF−CD74 complex.[12] The chemokine receptors CXCR2 and CXCR4, either alone or in a complex with CD74, also are activated by MIF leading to a variety of biological responses.[13−15] Given the upstream role of MIF in immunity, it is not surprising that various parasites encode their own MIF that binds to human CD74, dysregulating the immune response and promoting parasite survival.

Although a link among the enzymatic site, CD74 binding, and MIF biology is controversial, certain small molecule ligands that bind to the catalytic site form a MIF complex that functions as a CD74 antagonist, whereas other MIF−small molecule complexes have no effect on CD74 binding.[16,17] Virtual screening and optimization has been successful in identifying ligands that bind to the active site for human MIF.[18−22] In a recent study, the structure of *P. falciparum* MIF[3] was used for virtual screening of the enzymatic site with 2.1 million compounds to identify various inhibitors with low micromolar K_i values and used in structure−activity relationships (SAR) to develop more potent inhibitors.[23] In this study, we cocrystallized *Pf*MIF with two compounds identified from the virtual screen/optimization study.[23] These are the first *Pf*MIF−inhibitor complexes reported and may be used for development of novel therapeutics to treat malaria. The compounds in this study are 3-[(2-methyl-6-phenylpyridin-4-yl)oxy]phenol (**1**) and 4-(3-methoxy-5-methylphenoxy)-2-(4-methoxyphenyl)-6-methylpyridine (**2**) and have K_i values for inhibition of the 4-hydroxyphenylpyruvate tautomerase activity of 39 ± 8 and 38 ± 9 nM, respectively.[23]

Comparison of the *Pf*MIF−inhibitor structures with models of hMIF complexes reveals why these two compounds are selective for *Pf*MIF versus hMIF.[23] Finally, we present data indicating that one of these two inhibitors complexed to MIF is a potent antagonist of human CD74.

Received: May 12, 2014
Published: September 30, 2014

   dx.doi.org/10.1021/jm501168q | *J. Med. Chem.* 2014, 57, 8652−8656

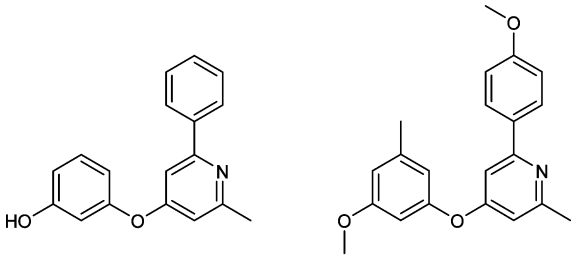

RESULTS AND DISCUSSION

Structural Analysis and Thermostability of *Pf*MIF. Cocrystallographic studies of *Pf*MIF complexed to either compounds **1** or **2** (Supporting Information (SI), Table S1) were performed to characterize the binding interactions between the small molecules and *Pf*MIF and elucidate the selectivity over hMIF. In contrast with the published apo-*Pf*MIF structure,[3] the protein in this study did not contain a poly-His tail at the C-terminal site. Both *Pf*MIF–inhibitor complexes were crystallized in a different space group ($I222$) than apo-*Pf*MIF ($P2_13$). X-ray data were collected to 3.02 and 2.87 Å for *Pf*MIF complexed to compounds **1** and **2**, and the structures were solved and refined to a R_{work}/R_{free} of 0.24/0.32 and 0.28/0.34, respectively. Comparison of the structures of the apo-*Pf*MIF and *Pf*MIF inhibitors indicated there were no global conformational changes. The root-mean-square (rms) deviation between the apo-*Pf*MIF and *Pf*MIF complexed to compounds **1** or **2** was 0.73 and 0.71 Å, respectively. Similar to apo-*Pf*MIF,[3] a few regions lacked electron density. These regions include the 60s loop and various C-terminal residues among the three subunits. Protein sequence alignment of the apo-*Pf*MIF and *Pf*MIF–inhibitor complexes with unmodelled residues (due to the lack of electron density) highlights that there are far more C-terminal residues missing in the apo-*Pf*MIF than the complexed structures (SI, Figure S1). The C-terminal region has roles in the integrity of the active site and the stability of the trimer, as β-strands from the C-terminal region intertwine with a β-sheet from an adjacent subunit and contribute to the seven-stranded β-sheet core of each monomer. The truncation of the C-terminal region in hMIF significantly decreases its catalytic activity and lowers the thermal denaturation of the trimer.[24,25] The thermostability of *Pf*MIF was measured by temperature-dependent circular dichroism (CD) (**1**) to examine the association between missing electron density for the C-terminal region (that indicates flexibility of this region) and reduction of *Pf*MIF tautomerase specific activity that is 20% of hMIF,[26] and (**2**) to determine whether stability of the trimer in complex with inhibitors is increased (SI, Figure S2A,B). It was surprising to find that the melting temperature (T_m) was 89 °C for apo-*Pf*MIF, 15 °C greater than the corresponding T_m of hMIF.[27] The T_m is not altered in the presence of the inhibitors. Analysis of *Pf*MIF to identify potential interactions responsible for this enhanced thermostability revealed interactions along the 3-fold axis as well as complementary electrostatic subunit–subunit interactions. There are three residues located along the solvent channel coincident with the 3-fold axis that form hydrogen bond interactions. The side chain carbonyl oxygen of Gln45 makes a hydrogen bond with the side chain nitrogen of Asn41 from an adjacent subunit. The side chain amide nitrogen of the same Gln45 makes a hydrogen bond with a carboxylate oxygen of Asp43 of the same adjacent subunit (Figure 1A,B). At the equivalent position of the hMIF structure, the trimer is stabilized by a hydrogen bond between the residue His40 of one subunit and Gln45 of another (SI, Figure S3A,B). Analysis of the *Pf*MIF subunit–subunit interface indicates a significant complementarity in electrostatic interactions (Figure 1C,D). In contrast, the subunit–subunit interface of hMIF is hydrophobic (SI, Figure S3C,D). It is difficult to quantitate the energies of these interactions, particularly for the buried complementary electrostatic potential at the subunit interface where the dielectric constant is low. However, these interactions are likely to increase thermostability of *Pf*MIF relative to hMIF. Thermostability is correlated to resistance to proteolysis,[28] suggesting that *Pf*MIF has evolved to preserve its structure and function in vivo to protect *Plasmodium falciparum* from the host immune response.

Interactions of *Pf*MIF with Compounds 1 and 2. The possibility that the compounds could fit into the initial electron density in two orientations was examined after refinement of the protein alone. "Opposite" orientations have been observed in hMIF.[29] The compounds were fit into electron density in each orientation, refined, and analyzed. In all instances, there were either clashes with active site residues or poor fitting with the opposite orientation (SI, Figure S4). Figure 2 displays the final coordinates of each compound with the corresponding electron density. Interactions between the *Pf*MIF active site and the two inhibitors were examined using PyMOL and LIGPLUS and calculated with CONTACT.[30] Analysis of the

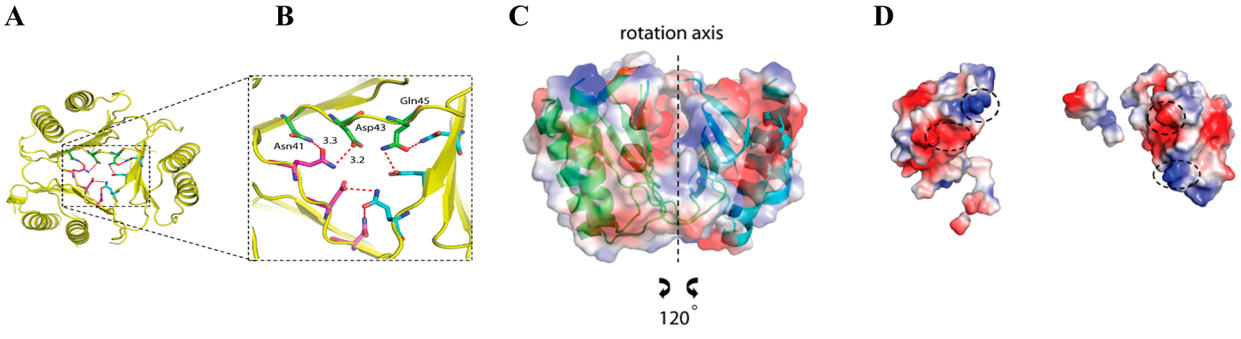

Figure 1. (A) Hydrogen bonding interactions in the opening of the solvent channel increase the stability of the trimer. (B) Gln45 makes two intersubunit hydrogen bonds with Asn41 and Asp43 for each monomer. (C) Illustration of the solvent exposed subunit–subunit interface. The rotation used was down the 3-fold axis to observe the electrostatic potential subunit–subunit interface. (D) The electrostatic potential map of the subunit–subunit interface shows strong electrostatic complementarity (dotted circles) between the two monomers. The positive and negative potentials are shown in blue and red, respectively.

dx.doi.org/10.1021/jm501168q | J. Med. Chem. 2014, 57, 8652–8656

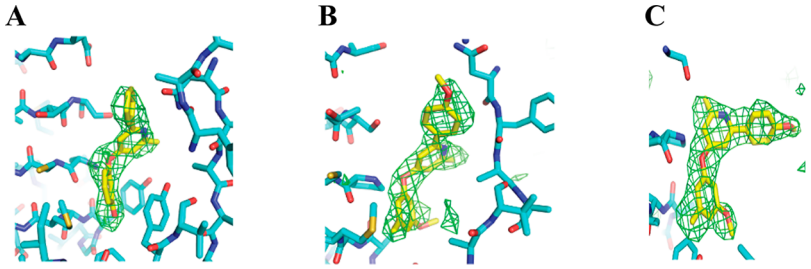

Figure 2. Experimental $F_o - F_c$ maps contoured at 3.0σ. (A) Compounds **1** and (B,C) **2** in the electron density at active sites of *Pf*MIF. **2** is in the same orientation but with different conformations at the two sites of *Pf*MIF. The inhibitors and *Pf*MIF are shown with yellow and cyan carbon atoms, respectively. Blue and red atoms are nitrogen and oxygen atoms, respectively.

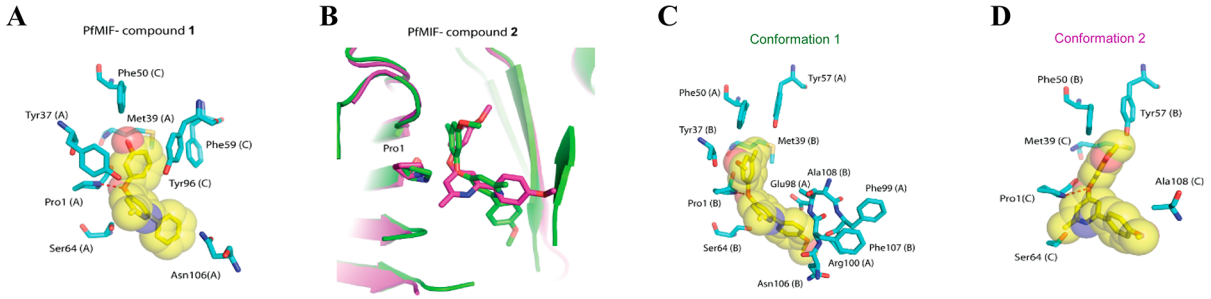

Figure 3. Interaction profile of **1** and **2** in the active sites of *Pf*MIF. Interacting residues were determined by ligplus (SI, Figure S5). Differences in the displayed residues for each active site are due to different interactions and to missing atoms (due to the absence of electron density) for some residues. The orientations of the compounds are based on superposition of each subunit and arranged with Pro-1 on the left of the compounds. (A) Interactions between the active site residues of *Pf*MIF and **1**. The compound is stabilized by an interaction between the biaryl ether oxygen of **1** and the nitrogen of Pro1 and aromatic−aromatic and van der Waals interactions of **1** with active site residues. (B) The two orientations of **2** in the active site of *Pf*MIF based on superposition of the protein atoms from the two subunits. (C,D) Interactions between the active site residues and **2** in its two orientations. Similar to *Pf*MIF−**1** interactions, **2** forms an interaction with nitrogen of Pro1 and a number of aromatic and van der Waals interactions with active site residues. The red dotted lines show the interaction between the biaryl ether and *Pf*MIF. For (A,C,D), yellow, red, and blue spheres are overlaid on the carbon, oxygen, and nitrogen atoms of each inhibitor, respectively.

interactions of compounds **1** and **2** with the active sites revealed two common features. In both *Pf*MIF complexes, the hydroxyphenyl ring of **1** and the 3-methoxy-5-methylphenyl ring of **2** are buried into the active site pocket, forming aromatic and van der Waals interactions. Although ether oxygens are not known for forming strong hydrogen bonds, we note that the biaryl ether oxygen of each compound forms a close contact with the nitrogen of Pro1 (Figure 3). The distance between the nitrogen of Pro1 and the biaryl ether oxygen of compound **1** is 2.4 Å (Figure 3A). The inhibitor also forms a number of aromatic and van der Waals interactions with residues Pro1, Tyr37, Met39, Ser64, and Asn106 of chain A and Phe50, Phe59, and Tyr96 of the adjacent subunit (chain C). In the *Pf*MIF−**2** complex, the inhibitor was found in two active sites in the same orientation but with different conformations (Figure 3B). Residues from asymmetric units did not affect either conformation for compound **2**. In the active site between chains A and B, the distance of the biaryl ether oxygen of compound **2** with Pro1 is 2.3 Å (Figure 3C), with the 3-methoxy-5-methylphenyl ring having aromatic and van der Waals interactions with Pro1, Tyr37, Met39, Ser64, Asn106, Phe107, and Ala108 of chain B and Phe50, Tyr57, Glu98, Phe99, and Arg100 of chain A. In the conformation of the active site that is located between chains B and C, the distance between the biaryl ether oxygen and the Pro1 nitrogen 2.6 Å. In this conformation, the 3-methoxy-5-methylphenyl ring makes aromatic and van der Waals interactions with Pro1, Met39, Ser64, and Ala108 of chain C and Phe50 and Tyr57 of chain B (Figure 3D). A ligplot shows the interactions between active site residues and inhibitors (SI, Figure S5).

Comparison of the crystallographic structures with the docking-based models from the virtual screen[23] shows significantly different conformations and interactions for the molecules in the active site (SI, Figure S6A−C). This is not surprising given the versatility to accept different conformations of a ligand in the active site of hMIF[29,31] and the dynamics of MIF as determined by NMR when some ligands bind to the active site.[31] This is also evident from the two conformations of compound **2** in separate *Pf*MIF active sites. Another complication of the original docking/optimization in the virtual screen was an imperfect target model created by using the C-terminal region of *Plasmodium berghei* MIF structure to compensate for the missing electron density for this region in the apo-*Pf*MIF structure.[23] Using the crystal structures of *Pf*MIF−inhibitor complexes, we repeated docking of **1** and **2**, focusing only in the active sites that are occupied by the inhibitors. The new docking-based models were significantly improved, with one orientation of compound **2** having significant superposition with the compound in the crystal structure (SI, Figure S6D−F).

Selectivity of Compounds 1 and 2 for *Pf*MIF versus hMIF. Biochemical experiments verified the selectivity of the two compounds for *Pf*MIF over hMIF.[23] To understand the structural basis of selectivity, the structures of hMIF (PDB entry 3DJH) and the *Pf*MIF complexes were superimposed using the secondary structure method (SSM).[30] The rms deviation of superimposed Cα atoms was 2.23 and 2.25 Å for

dx.doi.org/10.1021/jm501168q | J. Med. Chem. 2014, 57, 8652−8656

hMIF on *Pf*MIF complexed to compound **1** and **2**, respectively. The fairly high rms values are due to the low sequence identity (29%) between the two proteins (SI, Figure S7A). Comparison between modeled complexes of hMIF with both compounds reveals two common clashes, one with Ile64 and the second with Tyr95 from an adjacent subunit. Compound **1** in hMIF also clashes with Met2 and Met101 (SI, Figure S7B). The two methionine residues Met2 and Met101 that clash with compound **1** do not interfere with compound **2**. Instead, Val106 and Phe113 clash with compound **2** in the site between subunits A and B, and Phe113 clashes with compound **2** between chains B and C (SI, Figure S7C,D).

sCD74-*Pf*MIF Binding Assay. Some MIF–ligand complexes function as CD74 antagonists, while others do not.[16] Dose–response effects of compounds **1** and **2** on binding of *Pf*MIF to the human sCD74 revealed that compound **2** is more effective than **1** on inhibiting *Pf*MIF–receptor interactions (Figure 4). At the highest concentration for compound **2**, 75% of the *Pf*MIF–compound **2** is inhibited from binding sCD74. In contrast, compound **1** prevents binding of about 25% of *Pf*MIF at its highest concentration. Consistent with the lack of inhibition of hMIF by compounds **1** and **2**,[23] neither compound is found to inhibit the interaction of hMIF with sCD74. An emerging hypothesis related to disruption of MIF–CD74 emanates from a small structure–activity study of inhibitors of the hookworm-inducing parasite *Ancylostoma ceylanicum* macrophage migration inhibitory factor (*Ace*MIF).[16] In that study, it appeared that chemical moieties that protruded from the active site into the solvent were more effective at disrupting the *Ace*MIF–hCD74 interactions. In this study, one of the conformations of compound **2** has a chemical moiety outside the active site (SI, Figure S8), consistent with the hypothesis that MIF inhibitors with chemical groups outside the active site are more effective at disrupting MIF–receptor interactions. The structures from this study can be used to increase affinity to *Pf*MIF, increase inhibition of *Pf*MIF interactions with human CD74, and optimize for absorption, distribution, metabolism, and excretion (ADME) properties that are necessary for a therapeutic.

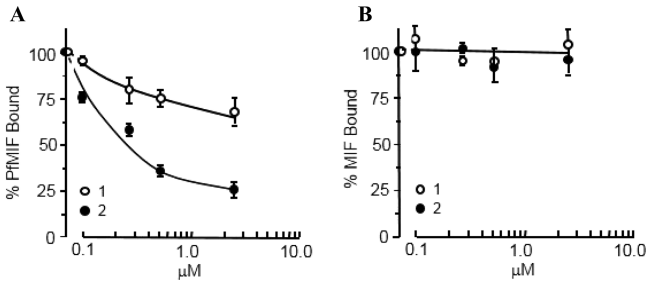

Figure 4. Effect of inhibitors **1** and **2** on (A) *Pf*MIF or (B) human MIF binding to the human ectodomain CD74 receptor (sCD74 = $CD74^{(his)}_6$114–232). Measured values are relative to diluent (DMSO) control for each concentration of inhibitor. Mean ± SD of four measurements.

■ ASSOCIATED CONTENT

Ⓢ Supporting Information

Methods, supporting figures, and the crystallographic table for *Pf*MIF complexed to compound **1** and **2**. This material is available free of charge via the Internet at http://pubs.acs.org.

Accession Codes

The atomic coordinates and structure factors for *Pf*MIF complexed to compound **1** (entry code 4P7M) and **2** (entry code 4P7S) have been deposited in the Protein Data Bank database.

■ AUTHOR INFORMATION

Corresponding Author

*Phone: 203-785-6233. Fax: 203-737-2027. E-mail: elias.lolis@yale.edu.

Author Contributions

All authors have given approval to the final version of the manuscript.

Notes

The authors declare no competing financial interest.

■ ACKNOWLEDGMENTS

We thank Markus K. Dahlgren for discussions concerning the modeled structure of ref [18]. Funded by NIH grant R01 AI065029, R01 AI110452, and R01 GM 32136.

■ ABBREVIATIONS USED

Pf, *Plasmodium falciparum*; MIF, macrophage migration inhibitory factor; 4-OT, 4-oxalocrotonate tautomerase; CHMI, 5-carboxymethyl-2-hydroxymucanate; OD, optical density; SAR, structure–activity relationship; rms, root-mean-square; CD, circular dichroism; T_m, melting temperature; *Pb*, *Plasmodium berghei*; sCD74, soluble CD74 ($CD74^{(his)}_6$114–232); TMB, tetramethylbenzidine; IPTG, β-D-1-thiogalactopyranoside; PBS-T, PBS/0.1% buffer Tween-20

■ REFERENCES

(1) Ariey, F.; Witkowski, B.; Amaratunga, C.; Beghain, J.; Langlois, A. C.; Khim, N.; Kim, S.; Duru, V.; Bouchier, C.; Ma, L.; Lim, P.; Leang, R.; Duong, S.; Sreng, S.; Suon, S.; Chuor, C. M.; Bout, D. M.; Menard, S.; Rogers, W. O.; Genton, B.; Fandeur, T.; Miotto, O.; Ringwald, P.; Le Bras, J.; Berry, A.; Barale, J. C.; Fairhurst, R. M.; Benoit-Vical, F.; Mercereau-Puijalon, O.; Menard, D. A molecular marker of artemisinin-resistant *Plasmodium falciparum* malaria. *Nature* **2014**, *505*, 50–55.

(2) Sun, T.; Holowka, T.; Song, Y.; Zierow, S.; Leng, L.; Chen, Y.; Xiong, H.; Griffith, J.; Nouraie, M.; Thuma, P. E.; Lolis, E.; Janse, C. J.; Gordeuk, V. R.; Augustijn, K.; Bucala, R. A Plasmodium-encoded cytokine suppresses T-cell immunity during malaria. *Proc. Natl. Acad. Sci. U. S. A.* **2012**, *109*, E2117–E2126.

(3) Dobson, S. E.; Augustijn, K. D.; Brannigan, J. A.; Schnick, C.; Janse, C. J.; Dodson, E. J.; Waters, A. P.; Wilkinson, A. J. The crystal structures of macrophage migration inhibitory factor from *Plasmodium falciparum* and *Plasmodium berghei*. *Protein Sci.* **2009**, *18*, 2578–2591.

(4) Kato, Y.; Muto, T.; Tomura, T.; Tsumura, H.; Watarai, H.; Mikayama, T.; Ishizaka, K.; Kuroki, R. The crystal structure of human glycosylation-inhibiting factor is a trimeric barrel with three 6-stranded beta-sheets. *Proc. Natl. Acad. Sci. U. S. A.* **1996**, *93*, 3007–3010.

(5) Sun, H. W.; Bernhagen, J.; Bucala, R.; Lolis, E. Crystal structure at 2.6 A resolution of human macrophage migration inhibitory factor. *Proc. Natl. Acad. Sci. U. S. A.* **1996**, *93*, 5191–5196.

(6) Suzuki, M.; Sugimoto, H.; Nakagawa, A.; Tanaka, I.; Nishihira, J.; Sakai, M. Crystal structure of the macrophage migration inhibitory factor from rat liver. *Nature Struct. Biol.* **1996**, *3*, 259–266.

(7) Subramanya, H. S.; Roper, D. I.; Dauter, Z.; Dodson, E. J.; Davies, G. J.; Wilson, K. S.; Wigley, D. B. Enzymatic ketonization of 2-hydroxymuconate: specificity and mechanism investigated by the crystal structures of two isomerases. *Biochemistry* **1996**, *35*, 792–802.

(8) Stivers, J. T.; Abeygunawardana, C.; Mildvan, A. S.; Hajipour, G.; Whitman, C. P.; Chen, L. H. Catalytic role of the amino-terminal

proline in 4-oxalocrotonate tautomerase: affinity labeling and heteronuclear NMR studies. *Biochemistry* **1996**, *35*, 803−813.
(9) Swope, M.; Sun, H. W.; Blake, P. R.; Lolis, E. Direct link between cytokine activity and a catalytic site for macrophage migration inhibitory factor. *EMBO J.* **1998**, *17*, 3534−41.
(10) Flieger, O.; Engling, A.; Bucala, R.; Lue, H.; Nickel, W.; Bernhagen, J. Regulated secretion of macrophage migration inhibitory factor is mediated by a non-classical pathway involving an ABC transporter. *FEBS Lett.* **2003**, *551*, 78−86.
(11) Merk, M.; Baugh, J.; Zierow, S.; Leng, L.; Pal, U.; Lee, S. J.; Ebert, A. D.; Mizue, Y.; Trent, J. O.; Mitchell, R.; Nickel, W.; Kavathas, P. B.; Bernhagen, J.; Bucala, R. The golgi-associated protein p115 mediates the secretion of macrophage migration inhibitory factor. *J. Immunol.* **2009**, *182*, 6896−6906.
(12) Shi, X.; Leng, L.; Wang, T.; Wang, W.; Du, X.; Li, J.; McDonald, C.; Chen, Z.; Murphy, J. W.; Lolis, E.; Noble, P.; Knudson, W.; Bucala, R. CD44 is the signaling component of the macrophage migration inhibitory factor-CD74 receptor complex. *Immunity* **2006**, *25*, 595−606.
(13) Mitchell, R. A.; Metz, C. N.; Peng, T.; Bucala, R. Sustained mitogen-activated protein kinase (MAPK) and cytoplasmic phospholipase A2 activation by macrophage migration inhibitory factor (MIF). Regulatory role in cell proliferation and glucocorticoid action. *J. Biol. Chem.* **1999**, *274*, 18100−6.
(14) Sampey, A. V.; Hall, P. H.; Mitchell, R. A.; Metz, C. N.; Morand, E. F. Regulation of synoviocyte phospholipase A2 and cyclooxygenase 2 by macrophage migration inhibitory factor. *Arthritis Rheum.* **2001**, *44*, 1273−1280.
(15) Onodera, S.; Nishihira, J.; Iwabuchi, K.; Koyama, Y.; Yoshida, K.; Tanaka, S.; Minami, A. Macrophage migration inhibitory factor up-regulates matrix metalloproteinase-9 and -13 in rat osteoblasts. Relevance to intracellular signaling pathways. *J. Biol. Chem.* **2002**, *277*, 7865−7874.
(16) Cho, Y.; Vermeire, J. J.; Merkel, J. S.; Leng, L.; Du, X.; Bucala, R.; Cappello, M.; Lolis, E. Drug repositioning and pharmacophore identification in the discovery of hookworm MIF inhibitors. *Chem. Biol.* **2011**, *18*, 1089−1101.
(17) Jorgensen, W. L.; Trofimov, A.; Du, X.; Hare, A. A.; Leng, L.; Bucala, R. Benzisothiazolones as modulators of macrophage migration inhibitory factor. *Bioorg. Med. Chem. Lett.* **2011**, *21*, 4545−4549.
(18) Cournia, Z.; Leng, L.; Gandavadi, S.; Du, X.; Bucala, R.; Jorgensen, W. L. Discovery of human macrophage migration inhibitory factor (MIF)-CD74 antagonists via virtual screening. *J. Med. Chem.* **2009**, *52*, 416−424.
(19) El-Turk, F.; Fauvet, B.; Ouertatani-Sakouhi, H.; Lugari, A.; Betzi, S.; Roche, P.; Morelli, X.; Lashuel, H. A. An integrative in silico methodology for the identification of modulators of macrophage migration inhibitory factor (MIF) tautomerase activity. *Bioorg. Med. Chem. 18*, 5425−5440.
(20) Orita, M.; Yamamoto, S.; Katayama, N.; Aoki, M.; Takayama, K.; Yamagiwa, Y.; Seki, N.; Suzuki, H.; Kurihara, H.; Sakashita, H.; Takeuchi, M.; Fujita, S.; Yamada, T.; Tanaka, A. Coumarin and chromen-4-one analogues as tautomerase inhibitors of macrophage migration inhibitory factor: discovery and X-ray crystallography. *J. Med. Chem.* **2001**, *44*, 540−547.
(21) Xu, L.; Li, Y.; Sun, H.; Zhen, X.; Qiao, C.; Tian, S.; Hou, T. Current developments of macrophage migration inhibitory factor (MIF) inhibitors. *Drug Discovery Today* **2013**, *18*, 592−600.
(22) Xu, L.; Zhang, Y.; Zheng, L.; Qiao, C.; Li, Y.; Li, D.; Zhen, X.; Hou, T. Discovery of novel inhibitors targeting the macrophage migration inhibitory factor via structure-based virtual screening and bioassays. *J. Med. Chem.* **2014**, *57*, 3737−3745.
(23) Dahlgren, M. K.; Garcia, A. B.; Hare, A. A.; Tirado-Rives, J.; Leng, L.; Bucala, R.; Jorgensen, W. L. Virtual screening and optimization yield low-nanomolar inhibitors of the tautomerase activity of *Plasmodium falciparum* macrophage migration inhibitory factor. *J. Med. Chem.* **2012**, *55*, 10148−10159.
(24) Swope, M. Cytokine, Hormone, or Enzyme: An Investigation of Biochemical and Biophysical Properties of Macrophage Migration Inhibitory Factor. Ph.D. Thesis. Yale University, New Haven, CT, 1998.
(25) El-Turk, F.; Cascella, M.; Ouertatani-Sakouhi, H.; Narayanan, R. L.; Leng, L.; Bucala, R.; Zweckstetter, M.; Rothlisberger, U.; Lashuel, H. A. The conformational flexibility of the carboxy terminal residues 105−114 is a key modulator of the catalytic activity and stability of macrophage migration inhibitory factor. *Biochemistry* **2008**, *47*, 10740−10756.
(26) Augustijn, K. D.; Kleemann, R.; Thompson, J.; Kooistra, T.; Crawford, C. E.; Reece, S. E.; Pain, A.; Siebum, A. H. G.; Janse, C. J.; Waters, A. P. Functional Characterization of the *Plasmodium falciparum* and *P. berghei* Homologues of Macrophage Migration Inhibitory Factor. *Infect. Immun.* **2007**, *75*, 1116−1128.
(27) Fan, C.; Rajasekaran, D.; Syed, M. A.; Leng, L.; Loria, J. P.; Bhandari, V.; Bucala, R.; Lolis, E. J. MIF intersubunit disulfide mutant antagonist supports activation of CD74 by endogenous MIF trimer at physiologic concentrations. *Proc. Natl. Acad. Sci. U. S. A.* **2013**, *110*, 10994−10999.
(28) Ahmad, S.; Kumar, V.; Ramanand, K. B.; Rao, N. M. Probing protein stability and proteolytic resistance by loop scanning: a comprehensive mutational analysis. *Protein Sci.* **2012**, *21*, 433−446.
(29) Crichlow, G. V.; Cheng, K. F.; Dabideen, D.; Ochani, M.; Aljabari, B.; Pavlov, V. A.; Miller, E. J.; Lolis, E.; Al-Abed, Y. Alternative chemical modifications reverse the binding orientation of a pharmacophore scaffold in the active site of macrophage migration inhibitory factor. *J. Biol. Chem.* **2007**, *282*, 23089−23095.
(30) The CCP4 suite: programs for protein crystallography. *Acta Crystallogr., Sect. D: Biol. Crystallogr.* **1994**, *50*, 760−763.
(31) Crichlow, G. V.; Fan, C.; Keeler, C.; Hodsdon, M.; Lolis, E. J. Structural interactions dictate the kinetics of macrophage migration inhibitory factor inhibition by different cancer-preventive isothiocyanates. *Biochemistry* **2012**, *51*, 7506−7514.